Journal of Alloys and Compounds 504 (2010) 224–227

Contents lists available at ScienceDirect

Journal of Alloys and Compounds

journal homepage: www.elsevier.com/locate/jallcom

A novel asymmetric hybrid supercapacitor based on Li_2FeSiO_4 and activated carbon electrodes

K. Karthikeyan [a], V. Aravindan [b], S.B. Lee [a], I.C. Jang [a], H.H. Lim [a], G.J. Park [c], M. Yoshio [c], Y.S. Lee [a,*]

[a] Faculty of Applied Chemical Engineering, Chonnam National University, Gwangju 500-757, Republic of Korea
[b] The Research Institute for Catalysis, Chonnam National University, Gwangju 500-757, Republic of Korea
[c] Department of Applied Chemistry, Saga University, Saga 840-8502, Japan

ARTICLE INFO

Article history:
Received 3 February 2010
Received in revised form 16 May 2010
Accepted 21 May 2010
Available online 1 June 2010

Keywords:
Li_2FeSiO_4
Cathode materials
Activated carbon
Hybrid supercapacitor
Energy density

ABSTRACT

A novel, hybrid supercapacitor is fabricated with Li_2FeSiO_4 (LFSO) as the negative electrode and activated carbon (AC) as the positive electrode in a standard, non-aqueous 1.0 M $LiPF_6$-EC/DMC electrolyte. The electrochemical properties of the LFSO/AC hybrid supercapacitor are investigated by means of cyclic voltammetry (CV), charge/discharge (C/D) measurement and electrochemical impedance spectroscopy (EIS). The CV results reveal the typical capacitance behavior of the LFSO/AC cell within the potential range of 0–3 V. The LFSO/AC cell presents a high discharge capacitance (D_{SC}) of 49 F g^{-1} at a current density of 1 mA cm^{-2} and delivers a specific energy of 43 Wh kg^{-1} and a specific power of 200 W kg^{-1}. The cell exhibits excellent cycleability and greater efficiency over 1000 cycles.

1. Introduction

The emergence of hybrid electric vehicles (HEVs) requires the development of new energy storage systems capable of delivering a higher power density and higher energy density. Two kinds of energy device are likely to be applied to most HEVs: secondary batteries [1,2], which have not been widely used in HEVs due to their low power density and short cycle life, and electrochemical supercapacitors (ECs) [3,4], which have higher power densities, shorter charge/discharge (C/D) times and longer cycle lives compared to secondary batteries. However, its low energy density remains an obstacle to its wide application in electric devices. Recently, the development of new power sources combining the advantages of both ECs and secondary batteries is attracting much interest. Two methods have been employed to develop such energy storage devices [5]: the combination of ECs and batteries, which, although offering high specific power, is complex and expensive, and the development of hybrid capacitors that contain a capacitor electrode and a battery electrode in a cell, which is called a hybrid supercapacitor. In a hybrid supercapacitor, the positive electrode stores the charge in a reversible, non-faradaic reaction of anions on the surface of an activated carbon (AC) material, whereas a reversible faradaic reaction occurs at the negative metal oxide electrode. This new, state-of-the-art, hybrid supercapacitor shows increased energy density, an excellent cycle life, and a high working voltage. Nowadays, the fabrication of hybrid supercapacitors with lithium intercalated compounds as the negative electrode and high surface AC as the positive electrode has been studied due to their higher specific energy than ECs. Amatucci et al. [6] and Pasquier et al. [7] have developed a non-aqueous hybrid system with $Li_4Ti_5O_{12}$ anode. Furthermore, Wang et al. [8,9] have reported $LiMn_2O_4$ and $LiCo_{1/3}Ni_{1/3}Mn_{1/3}O_2$ as the negative electrode for hybrid supercapacitors in an aqueous system. Vasanthi et al. [10] also have utilized olivine-type cathode material ($LiCoPO_4$) for hybrid supercapacitors in a non-aqueous electrolyte. However, none of the electrode materials reported in literature exhibited the long term cycleability except $Li_4Ti_5O_{12}$. All the materials studied were experienced the severe capacity fading during the cycling with both activated carbon or carbon nanotubes and thermal stability is also questionable. In order to circumvent these issues, polyanionic framework materials ($(XO_4)^{n-}$, X = P, Si, As, Mo or W) were studied as possible electrode materials for supercapacitor as well as lithium battery applications. These materials were attracted by the researchers due to their appealing properties like structural, electrochemical and thermal stability and eco friendliness, among them, silicates and phosphates are noteworthy. Further, a very few reports (mentioned previously) could be traced for lithiated cathodes used as electrode materials for non-aqueous supercapacitor applications.

In addition, metal orthosilicate (Li_2MSiO_4, M = Fe and Mn)-based cathode materials are attracting much attention for lithium

* Corresponding author. Tel.: +82 62 530 1904; fax: +82 62 530 1909.
E-mail address: leeys@chonnam.ac.kr (Y.S. Lee).

0925-8388/$ – see front matter © 2010 Elsevier B.V. All rights reserved.
doi:10.1016/j.jallcom.2010.05.097

battery applications because of their intrinsic thermal and structural stability, natural abundance, environmental benign and cost effectiveness [11–13]. They also have relatively higher lithium ion mobility, better thermal properties, higher energy density and higher theoretical capacity (>300 mAh g^{-1}) than conventional cathode materials. In the orthosilicates family, especially Li_2FeSiO_4 (LFSO) has been distinguished the removal of two-electron per unit formula is possible [11,12]. Additionally, this material generally allows a wide range of solid solution with various compositions and species. Among them, LFSO is an exciting platform for the development of next-generation cathode materials for lithium secondary batteries. To the best of our knowledge, no research has been reported on the utilization of lithium iron silicates as the electrode material for hybrid supercapacitors. In this work, therefore, we have prepared nanosized LFSO material by solid-state reaction method. An asymmetric hybrid supercapacitor was assembled using the prepared LFSO material as the negative electrode and AC as the positive electrode. The electrochemical and cycling performances of this hybrid supercapacitor were investigated in 1 M $LiPF_6$-EC/DMC electrolyte system.

2. Experimental

LFSO was prepared by solid-state reaction method. LiOH (Junsei, Japan), $FeC_2O_4{\cdot}2H_2O$ (Junsei, Japan), SiO_2 (Junsei, Japan) and adipic acid (Aldrich, USA) were used as the starting materials. Adipic acid (0.2 M) was added as a carbon source to improve the electric conductivity between particles by carbon coating. A stoichiometric amount of starting materials with adipic acid was ground well and heated at 400 °C for 4 h in air. After cooling down to room temperature, the mixture was ground again, pelletized and finally calcined at 800 °C for 12 h under argon atmosphere.

The phase analysis of the resultant sample was characterized by an X-ray diffractometer (XRD, Rint 1000, Rigaku, Japan) with Cu-Kα as the radiation (λ = 1.5405 Å). The surface morphology of the sample was investigated by a scanning electron microscope (SEM, S-4700, Hitachi, Japan). Electrochemical performances were analyzed with a coin-type cell assembled using AC (1676 m^2/g of specific surface area) as the cathode and LFSO as the anode. The electrodes were prepared by pressing the slurry of a mixture composed of 70 wt% active material (AC for the cathode, LFSO for the anode), 20 wt% conducting agent (Ketjen black) and 10 wt% binder (teflonized acetylene black) onto a stainless steel mesh and then drying it at 160 °C for 4 h in a vacuum oven. The diameter of the electrode was 200 mm^2. The mass ratio of anode to cathode was about 1:2. The cells were assembled in an argon-filled glove box by pressing LFSO anode, porous polypropylene separator (celgard 3401) and an AC cathode. The 1 M $LiPF_6$-EC/DMC was used as the electrolyte solution. Cyclic voltammetry (CV) and electrochemical impedance spectroscopy (EIS) studies were performed by using an electrochemical analyzer (SP-150, Bio-Logic, France). Charge-discharge testing was carried out between a cell voltage of 0–3 V at the current density of 1 mA cm^{-2} by using a battery cycle tester (WBCS 3000, Won-A-Tech, Korea). The capacitance (F) of the hybrid cell was calculated as follows:

$$C_{cell} = \frac{I}{dV/dt},$$

where I is the current density (mA cm^{-2}), t the discharge time (s), and C_{cell} the total capacitance (F). The discharge capacitance (D_{SC}) in F g^{-1} is [14,15]:

$$C_S = \frac{4C_{cell}}{M} \quad (1)$$

where M is the total weight (g) of the two electrode materials.

3. Results and discussion

Fig. 1 presents the XRD pattern of the synthesized LFSO material. The well-developed and narrow XRD peak reveals the good crystallinity of the prepared LFSO. There was no trace of unreacted starting materials and no iron oxide phases remained in the powders except a small amount of Li_2SiO_3 phase in the diffractogram. The crystal system of LFSO could be indexed to the orthorhombic structure with a space group *Pmn*2 [16]. The degree of the crystallinity of LFSO, i.e., the shape and size of the particles, was examined by XRD and SEM. The crystalline size (δ) of the prepared

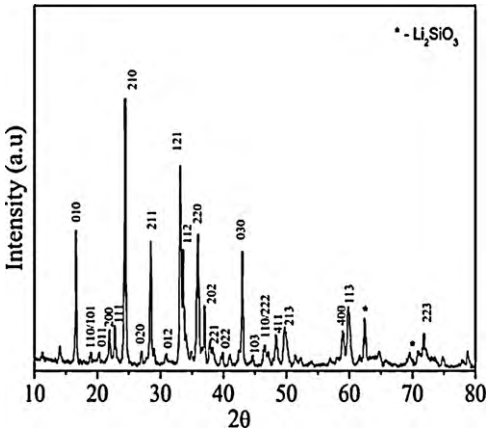

Fig. 1. XRD pattern of Li_2FeSiO_4 calcined at 800 °C for 12 h in air atmosphere.

LFSO powder was calculated by using Scherrer's formula:

$$\delta = \frac{0.9\lambda}{\beta \cos\theta}$$

where λ s the wavelength of the X-ray radiation (Cu Kα = 0.15418 nm) and β the line width at half maximum height at the diffraction angle of θ. The average crystallite size of powders grown by solid-state reaction was found 62 nm. The shape and surface morphology of LFSO particles were observed by SEM analysis.

Fig. 2 presents two SEM images at different magnifications of the LFSO powder obtained at 800 °C for 12 h. The LFSO powders consist

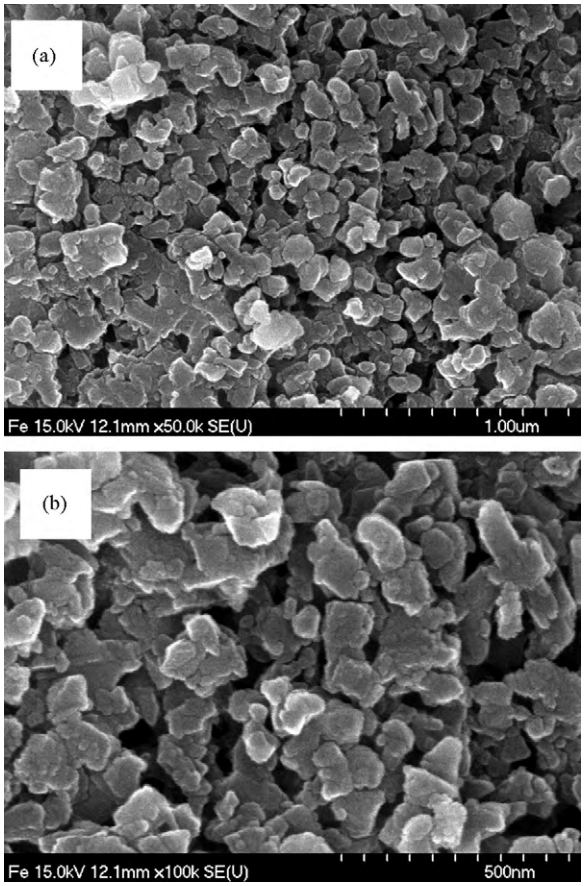

Fig. 2. SEM images of the as-prepared Li_2FeSiO_4 particles at (a) 50,000× and (b) 100,000× magnifications.

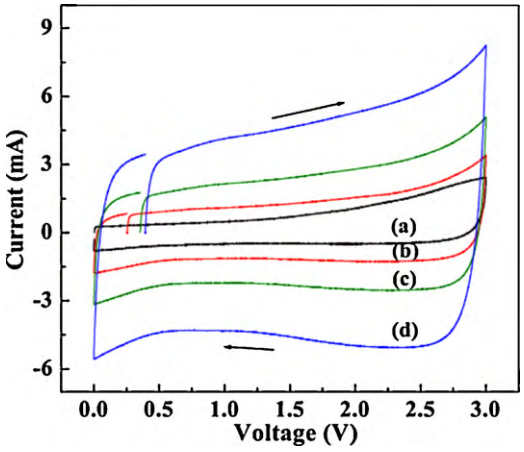

Fig. 3. Cyclic voltammograms of the LFSO/AC cell at different scan rates.

of well-developed particles with narrow and uniform particle size distribution. From the images, the average particle size of the prepared material was estimated to be 50–75 nm, which was in good agreement with the XRD data.

The capacitive performance of the prepared LFSO cell was measured by CV testing. Fig. 3 presents the *I–V* curves of LFSO/AC between the potential of 0–3 V at different scan rates. The rectangular-like behavior of the CV curves in Fig. 3 demonstrates the good capacitive behavior and high reversibility of LFSO/AC. The curve retains a good rectangular-like shape even at a high scan rate of 20 mV s^{-1}. The CV result also reveals that the hybrid cell is highly stable in 1 M $LiPF_6$/EC:DMC electrolyte within the observed potential range. The LFSO anode depends on electron transfer to generate pseudocapacitance. Li^+ is absorbed on the AC surface during the charging state and de-absorbed from the AC surface during the discharging state. The cathode utilizes an electrochemical double layer mechanism to realize energy storage. The following equations explain the possible charge storage mechanism of LFSO/AC:

$$\text{Anode}: \ Li_2{}^{+}Fe^{2+}SiO_4 \Leftrightarrow Li_{1-x}{}^{+}Fe^{3+}SiO_4 + (1+x)Li^+ + xe^-$$

$$\text{Cathode}: AC + (1+x)Li^+ + xe^- \Leftrightarrow AC(xe^-) + \ //(1+x)Li^+ \ (//\text{stands for double layer})$$

The specific capacitance (SC) was calculated from the CV curves by using the following relation:

$$C_{SC} = \frac{I}{s \times m}$$

where *I* is the current density in A, s the scan rate in mV s^{-1} and m the mass of the active materials. SCs of 58, 43, 41 and 36 F g^{-1} were obtained at scan rates of 2, 5, 10 and 20 mV s^{-1}, respectively. This decrease in SC with increasing scan rate was attributed to the reduced diffusion rate of the ions in the pores at higher scan rates [17]. The increase in scan rate directly reduced the ion diffusion, since at high scan rates the ions approach only the outer surface of the electrode material.

Electrochemical analyses of LFSO/AC in 1 M $LiPF_6$-EC/DMC were undertaken from 0 to 3 V at various current densities. Fig. 4(a) shows the C/D curve of the LFSO/AC hybrid cell at a current density of 1 mA cm^{-2}. The linear and symmetrical feature exhibited by the C/D curves indicates an excellent electrochemical reversibility and a good capacitance behavior of the LFSO/AC cell. A potential jump/drop was observed at the beginning of the charge and discharge, which is associated with ohmic drop. The magnitude of this jump/drop increased with increasing current density. The C/D

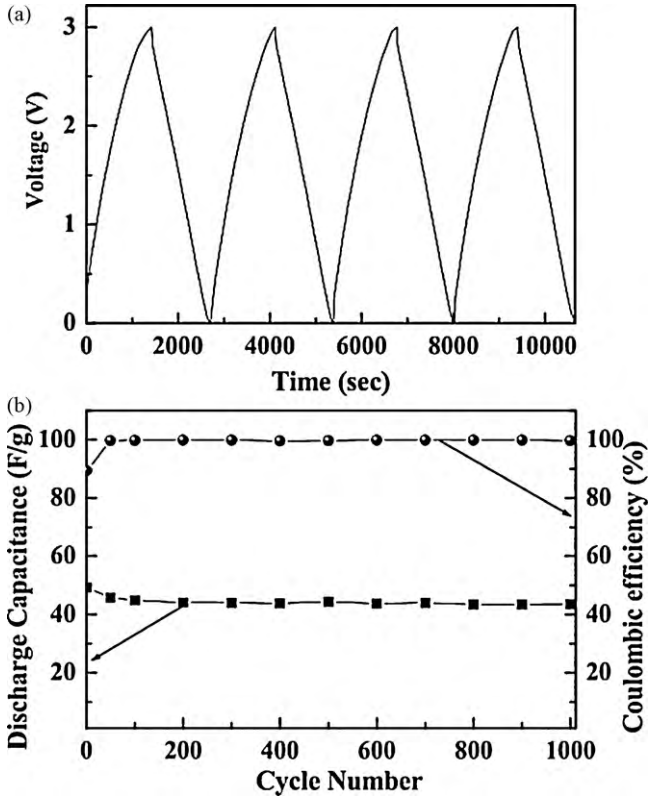

Fig. 4. (a) Charge/discharge curves and (b) cycleability and columbic efficiency of LFSO/AC at a current density of 1 mA cm^{-2}.

curves also revealed the low ohmic drop of the LFSO/AC cell. The average internal resistance (R) of the hybrid cell was calculated according to the following formula:

$$R = \frac{V_{charge} - V_{discharge}}{2I} \quad (2)$$

where V_{charge} and $V_{discharge}$ are the potentials at the end of charging and at the beginning of discharging, respectively and *I* is the applied current. The *R*-value for the LFSO/AC cell was calculated to be 58 Ω, which reflects both the non-optimized contacts between the electrodes and the current collectors and the solution resistance. The D_{SC} from the C/D studies was calculated by using Eq. (1). The D_{SC} of 50 F g^{-1} was obtained at a current density of 1 mA cm^{-2}. Fig. 4(b) shows the cyclability and coulombic efficiency of the LFSO/AC cell. The hybrid cell clearly exhibits a very small D_{SC} fade during long-term cycling. The D_{SC} of the hybrid cell decreased by only 12% from 49.5 F g^{-1} in the first cycle to 44 F g^{-1} after 1000 cycles, due to detachment and dissolution of the active material and reduction of active sites in LFSO. The good reversibility with a coulombic efficiency higher than 99% demonstrated the excellent capacitive property of the LFSO/AC cell. The

Fig. 5(a) presents the dependence of D_{SC} on the current density. As shown in Fig. 4(b), D_{SC} decreased from 49 to 39 F g^{-1} as the current density increased from 1 to 7 mA cm^{-2}, which was attributed to the lower utilization of active materials (as lithium ions do not have enough time to enter into the core of the material) due to the strong polarizations at higher current density [18]. Fig. 5(b) demonstrates the capability of LFSO/AC in 1 M $LiPF_6$ EC/DMC to deliver high power performance. For example, an energy density of 43 Wh kg^{-1} was obtained at a power density of 200 W kg^{-1} and at a power density of 1400 W kg^{-1}, the energy density was retained at 33 Wh kg^{-1}. The power and energy density limitations at high rates are associated with the complex resistance and indirect diffusion pathways within the textures. At high discharge current, only the

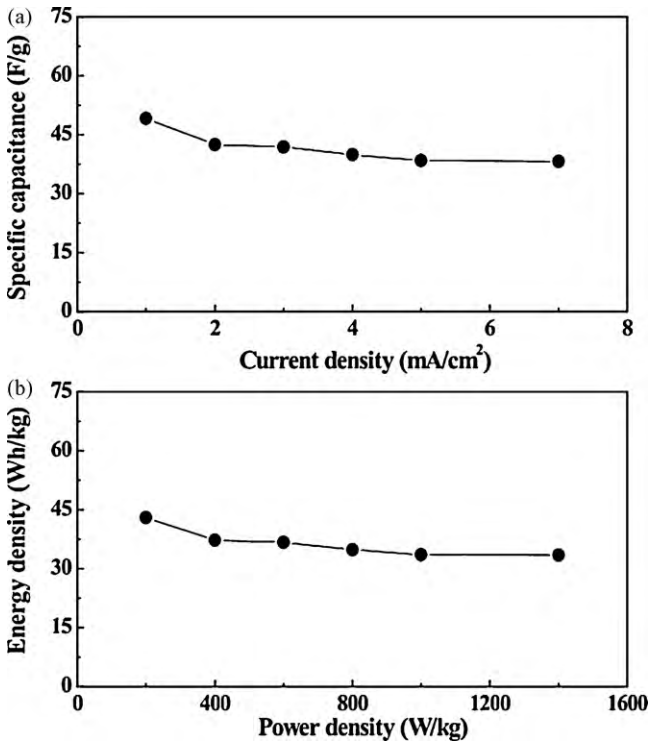

Fig. 5. (a) Discharge capacitance (D_{SC}) at various current densities and (b) Ragone's plot of the LFSO/AC cell.

outer regions of the electrode surface can be accessed by the ions, whereas at the low current, both the outer and the inner surfaces are used for charge storage. The good power and energy performances of LFSO/AC confirmed the effective utilization of most of the surfaces for the charge storage.

EIS is a powerful tool to investigate the penetration of current into the surface of the electrode and determine the degree to which ions access through the surface at specific frequencies. Fig. 6 shows the EIS spectra of the LFSO/AC cell over the frequency range from 100 kHz to 100 mHz at open circuit voltage. The EIS diagram shows a distorted semi-circle in the high frequency region and an inclined line in the low frequency region. In the former, the intercept of the semicircle represents the solution resistance (R_{sol}) and the diameter of the semicircle represents the resistance

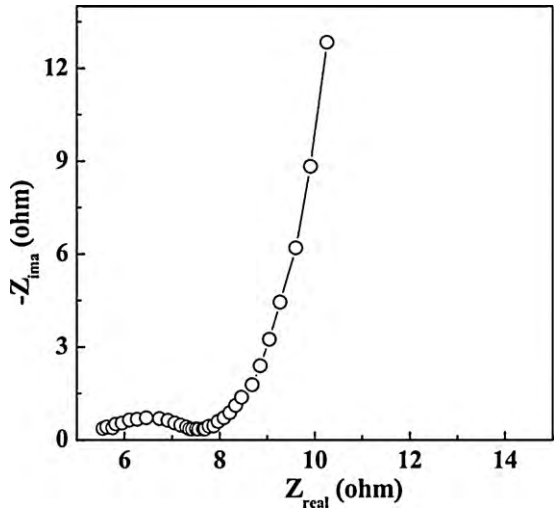

Fig. 6. EIS spectra of the LFSO/AC cell at open circuit voltage.

of the charge transfer. R_{ct} represents the sum of the resistance offered to Li^+ migration through the bulk of the electrode, the electrode/electrolyte resistance, and the electrode resistance. The EIS spectra demonstrated the good ionic conductivity and low resistance of LFSO/AC in 1.0 M $LiPF_6$ EC/DMC. Lowering the resistance increases the current on the electrode surface, which enhances the diffusing rate of the Li^+ ions toward the electrode and thus increases the electrochemical performance. In the low frequency region, the line close to 90° was attributed to the capacitive behavior. The SC of the hybrid cell from the EIS spectra was calculated by the following formula:

$$C = -\frac{1}{2}\pi f Z_{im} m$$

where f is the frequency (Hz), Z_{im} is the imaginary part of resistance (Ω) and m is the mass of the active materials. The SC value of 56 F g^{-1} obtained for the hybrid cell was slightly different from that obtained from the CV and C/D studies, possibly due to the penetration of alternate current into the electrode bulk with more hindrance [19].

4. Conclusion

A 3 V asymmetric hybrid capacitor was fabricated with LFSO as the negative electrode and AC as the positive electrode (LFSO/AC). This hybrid cell delivered a discharge SC of 49 F g^{-1} at a current density of 1 mA cm^{-2}. After 1000 cycles, the LFSO/AC cell exhibited an excellent cycling performance with an efficiency of more than 99.5%. A specific energy of 43 Wh kg^{-1} and specific power of 200 W kg^{-1} were obtained based on the total weight of the active materials. The hybrid cell also demonstrated a high rate performance and stable electrochemical properties within the potential range of 0–3 V in the standard, non-aqueous electrolyte solution.

Acknowledgements

This work was supported by Priority Research Centers Program through the National Research Foundation of Korea (NRF) funded by the Ministry of Education, Science and Technology (2009-0094058)

References

[1] A. Cooper, J. Power Sources 133 (2004) 116–125.
[2] N. Sato, J. Power Sources 99 (2001) 70–77.
[3] M.W. Verbrugge, P. Liu, J. Electrochem. Soc. 153 (2006) A1237–A1245.
[4] B.E. Conway, W.G. Pell, J. Solid State Electrochem. 7 (2003) 637–644.
[5] G. Sikha, R.E. White, B.N. Popov, J. Electrochem. Soc. 152 (2005) A1682–A1693.
[6] G.G. Amatucci, J.M. Tarascon, L.C. Klein, J. Electrochem. Soc. 143 (1996) 1114–1123.
[7] A.D. Pasquier, I. Plitz, J. Gural, F. Badway, G.G. Amatucci, J. Power Sources 136 (2004) 160–170.
[8] Y.G. Wang, Y.Y. Xia, J. Electrochem. Soc. 153 (2006) A450–A454.
[9] Y.G. Wang, J.Y. Luo, C.X. Wang, Y.Y. Xia, J. Electrochem. Soc. 153 (2006) A1425–A1431.
[10] R. Vasanthi, D. Kalpana, N.G. Renganathan, J. Solid State Electrochem. 12 (2008) 961–969.
[11] R. Dominko, M. Bele, M. Gaberscek, A. Meden, M. Remskar, J. Jamnik, Electrochem. Commun. 8 (2006) 217–222.
[12] A. Nyten, A. Abouimrane, M. Armand, T. Gustaffson, J.O. Thomas, Electrochem. Commun. 7 (2005) 156–160.
[13] K. Karthikeyan, V. Aravindan, S.B. Lee, I.C. Jang, H.H. Lim, G.J. Park, M. Yoshio, Y.S. Lee, J. Power Sources 195 (2010) 3761.
[14] J.H. Park, O.O. Park, J. Power Sources 111 (2002) 185–190.
[15] V. Khomenko, E.R. Pinero, F. Beguin, J. Power Sources 153 (2006) 183–190.
[16] C. Keffer, A. Mighell, F. Mauer, H. Swanson, S. Block, Inorg. Chem. 6 (1967) 119–125.
[17] D. Kalpana, K.S. Omkumar, S. Suresh Kumar, N.G. Renganathan, Electrochim. Acta 52 (2006) 1309–1315.
[18] K. Zaghib, J.B. Goodenough, A. Mauger, C. Julien, J. Power Sources 194 (2009) 1021–1023.
[19] W. Xing, S.Z. Qiao, R.G. Ding, F. Li, G.Q. Lu, Z.F. Yan, H.M. Cheng, Carbon 44 (2006) 216–224.